

N 9 1 - 2 8 0 8 6 4

## KAON - NUCLEUS SCATTERING

Byungsik Hong, Warren W. Buck and Khin M. Maung  
Department of Physics  
Hampton University  
Hampton, Virginia

Technical Monitors  
John W. Wilson and L.W. Townsend  
NASA Langley Research Center  
Hampton, Virginia

53-72  
56604  
P-16

### ABSTRACT

Two kinds of number density distributions of the nucleus, harmonic well and Woods-Saxon models, are used with our  $t$ -matrix that is taken from the scattering experiments to find a simple optical potential. The parameterized two body inputs, which are kaon-nucleon total cross sections, elastic slope parameters, and the ratio of the real to imaginary part of the forward elastic scattering amplitude, are shown. The eikonal approximation was chosen as our solution method to estimate the total and absorptive cross sections for the kaon-nucleus scattering.

## KAON - NUCLEUS SCATTERING

For the scattering of the high energy incoming particle, particularly a meson, by a nucleus, it is expected that the situation can be considered in terms of its scattering by the constituent nucleons of the nucleus individually. This means the many body problem may be reduced to a collection of the two body interactions.

One of the successful scattering frameworks is the multiple scattering theory. A simple picture of the scattering of elementary particles by a nucleus is to view the scattering in terms of the projectile interactions with each single constituent of the nucleus (single scattering). There may be other terms contributing to the scattering such as the projectile interacting with two consecutive constituents (double scattering). Similarly there are contributions from three, four, and more successive scatterings. The formalisms using this picture are called multiple scattering theories.<sup>1,2,3</sup> It is clear from this description that the scattering from a nucleus is determined from the amplitude for the scattering of the projectile from a single target constituent, i.e., a two body scattering amplitude.<sup>4</sup>

A general multiple scattering theory for scattering between two nuclei (neglecting three body interaction) has previously been developed by Wilson.<sup>4,5</sup> The reaction for the heavy ion projectile which is the previous application of Wilson's theory was well developed by Wilson et al.<sup>6</sup> And the application to the antiproton, antideuteron and antinuclei was also done by Buck et al.<sup>7</sup> giving good agreement with the available experimental data.

A successful feature of multiple scattering theories manifests itself when combined with the optical model. This allows the optical potential for elementary particle scattering from a nucleus to be determined from more fundamental quantities such as the two body scattering amplitude and the target number density function.

$$W(R) = A \int d^3r' \rho_A(\mathbf{r}') t(e, \mathbf{r}' - \mathbf{R}) \quad (1)$$

where  $R$  is the distance between the origin and projectile particle,  $r'$  is the separation between the origin and the considered target constituent,  $A$  is the target mass number,  $e$  is the kaon-nucleon kinetic energy in the center of the mass frame,  $\rho_A$  is the target number density, and  $t$  is the energy dependent kaon-nucleon transition amplitude obtained from scattering experiments. The origin was taken at the center of the mass of the target nucleus. In the eikonal context, the scattering amplitude for the kaon-nucleus scattering is given by

$$f(k, \theta) = \frac{k}{2\pi i} \int d^2b e^{i\mathbf{q} \cdot \mathbf{b}} [e^{i\chi(\mathbf{b}, k)} - 1] \quad (2)$$

where

$$\chi(\mathbf{b}, k) = -\frac{1}{2k} \frac{2\mu}{\hbar^2} \int_{-\infty}^{\infty} W(\mathbf{b}, z) dz \quad (3)$$

is the eikonal scattering phase shift function,  $b$  is the impact parameter, and  $\mu$  is the reduced mass of the  $K$ -nucleus system. Using the above scattering amplitude and the optical theorem, we can obtain the total and absorption cross section expressed as follows:

$$\sigma_{total} = 2 \int d^2b [1 - e^{Im_\chi(\mathbf{b},k)} \cos(Re_\chi(\mathbf{b},k))] \quad (4)$$

and

$$\sigma_{absorption} = \int d^2b [1 - e^{-2Im_\chi(\mathbf{b},k)}]. \quad (5)$$

The number density  $\rho_A$  of nuclear matter can be extracted from the corresponding charge density  $\rho_C$  by assuming <sup>7</sup>

$$\rho_C(r) = \int \rho_N(r') \rho_A(r+r') d^3r' \quad (6)$$

where  $\rho_C$  is the nuclear charge distribution,  $\rho_N$  is the nucleon charge distribution, and  $\rho_A$  is the nuclear single particle density.  $\rho_N$  was taken to be the usual Gaussian function

$$\rho_N(r) = \left(\frac{3}{2\pi r_N^2}\right)^{3/2} \exp\left(-\frac{3r^2}{2r_N^2}\right) \quad (7)$$

with the nucleon root-mean-square charge radius set equal to the proton value of  $0.87fm^{12}$ .

For nuclei with  $A < 20$  we used an harmonic well form of  $\rho_C$  as

$$\rho_C(r) = \rho_0 [1 + \gamma \left(\frac{r}{2}\right)^2] \exp\left(-\frac{r^2}{a^2}\right) \quad (8)$$

with the charge distribution parameters  $\gamma$  and  $a$  listed in Table I. Substituting Eq.(7) and Eq. (8) into Eq.(6), we get

$$\rho_A(r) = \frac{\rho_0 a^3}{8s^3} \left[1 + \frac{3\gamma}{2} - \frac{3\gamma a^2}{8s^2} + \frac{\gamma a^2 r^2}{16s^4}\right] \exp\left(-\frac{r^2}{4s^2}\right) \quad (9)$$

where

$$s^2 = \frac{a^2}{4} - \frac{r_N^2}{6}. \quad (10)$$

For target nuclei with  $A \geq 20$  we choose a Woods-Saxon form of charge distribution

$$\rho_C(r) = \rho_0 \left[1 + \exp\left(\frac{r-R}{c}\right)\right]^{-1} \quad (11)$$

where the parameters  $R$  and  $c$  are given by

$$R = r_{0.5} \quad (12)$$

and

$$c = \frac{t_c}{4.4} \quad (13)$$

and  $r_{0.5}$  is the radius at half-density with  $t_c$  representing the skin thickness. Values for  $R$  and  $t_c$  are also shown in table I. If we substitute Eqs. (7) and (11) into Eq. (6), we'll see the nuclear single particle density that is also of Woods-Saxon form with the same  $R$ , but different normalization coefficient,  $\rho_0$ , and surface thickness. The latter is given (in  $fm$ ) by

$$t_A = [5.08r_N \ln(\frac{3\beta - 1}{3 - \beta})]^{-1} \quad (14)$$

and

$$\beta = \exp(2.54 \frac{r_N}{t_c}). \quad (15)$$

We choose the kaon-nucleon scattering amplitude to be the function of momentum transfer  $q$  as

$$f(q) = \frac{k}{4\pi} \sigma_T (i + \alpha) e^{-Bq^2/2} \quad (16)$$

where  $k$  is the wave number of the kaon-nucleon system,  $\sigma_T$  is the kaon-nucleon total cross section,  $\alpha$  is the ratio of the real to imaginary part of the forward elastic scattering, and  $B$  is the slope parameter. Then the  $t$ -matrix in the coordinate space is

$$t(r) = -\sqrt{\frac{e\hbar^2}{2\mu'}} \sigma_T (i + \alpha) \frac{1}{(2\pi B)^{3/2}} e^{-r^2/(2B)} \quad (17)$$

where  $e$  is the total kinetic energy in the c.m. frame and  $\mu'$  is the reduced mass of the colliding particles. We compared our scattering amplitude, Eq. (16), with the experimental data of the  $K^+p$  differential cross section taken from Ref.13 and show the results in Figs. 1 and 2. In the case of the kaon-nucleus scattering, the comparison to our calculation utilizing eikonal scattering amplitude, Eq. (2), with the experimental data<sup>9</sup> for  $C^{12}$  are displayed in Figs. 3 and 4. The optical potentials coming from the above informations for  $K^+$  and  $K^-$  projectiles and  $C^{12}$  target are shown in Figs. 5 and 6.

The total cross sections of the  $K^\pm$ -proton system may be fitted by the following form:

$$\sigma_T = \sigma_b (P_K^{Lab}) + \sum_i g_i (P_K^{Lab}) \quad (18)$$

where  $P_K^{Lab}$  is the corresponding kaon laboratory momentum in  $GeV/c$  and the unit of  $\sigma$  is mb. The typical form of  $g_i (P_K^{Lab})$  is that

$$g_i (P_K^{Lab}) = \frac{m_i}{[(P_{R_i} - P_K^{Lab}) \frac{2}{n_i}]^2 + 1} \quad (19)$$

where  $P_{R_i}$  is the resonance momentum of the  $i$ th peak and  $m_i$  and  $n_i$  are the constants which have to be determined from the data.

Eq. (18) actually corresponds to the superposition of Breit-Wigner formulae where  $\sigma_b (P_K^{Lab})$  is a non-resonant background. Our fitting constants in the resonance energy range are displayed in table II. The background functions are fitted by

$$\sigma_b (P_K^{Lab}) = 23.2e^{-0.003P_K^{Lab}} \quad (20)$$

for  $K^- p$  scattering and

$$\sigma_b (P_K^{Lab}) = 16.8 - \frac{1}{P_K^{Lab}} \quad (21)$$

for  $K^+ p$  scattering. When  $P_K^{Lab}$  is less than 0.7 GeV/c in  $K^- p$  scattering, we used the following function:

$$\sigma_T = 172.38e^{-2.0(P_K^{Lab} + 0.1)} \quad (22)$$

In the more high energy region, the empirical formulae for  $Kp$  system are given by

$$\sigma_T = 20.18 + \frac{24.63}{P_K^{Lab}} \quad (23)$$

when  $P_K^{Lab} > 20\text{GeV}/c$  in  $K^- p$  system and

$$\sigma_T = 16.8 - \frac{0.22}{P_K^{Lab}} \quad (24)$$

when  $P_K^{Lab} > 5\text{GeV}/c$  in  $K^+ p$  system.

The fitting formulae which we used for  $K^\pm - N$  systems are Eq. (25) through (28). For  $K^- n$  scattering,

$$\sigma_T = -1033.0 + 1060.0P_K^{Lab-0.03} + 28.0\ln P_K^{Lab} \quad (25)$$

when  $P_K^{Lab} \geq 2.5\text{GeV}/c$  and

$$\sigma_T = 23.91 + 17.0e^{-(P_K^{Lab} - 1.0)^2/0.12} \quad (26)$$

when  $P_K^{Lab} < 2.5\text{GeV}/c$ . And for  $K^+ n$  scattering,

$$\sigma_T = 18.4 + 175.0P_K^{Lab-7.85} + 0.2\ln^2 P_K^{Lab} - 0.75\ln P_K^{Lab} \quad (27)$$

when  $P_K^{Lab} \geq 2.5 GeV/c$  and

$$\sigma T = \alpha (18.0 + 3.0e^{-(P_K^{Lab} - 1.2)^2/0.08}) \quad (28)$$

when  $P_K^{Lab} < 2.5 GeV/c$ . The constant  $\alpha$  is equal to 1 when  $P_K^{Lab} \geq 1.2 GeV/c$  and 0.94 when  $P_K^{Lab} < 1.2 GeV/c$ .

We determined the fitting formulae of slope parameter,  $B$ , in the range of  $0.1 \leq |t| \leq 0.4 (GeV/c)^2$ . The resultant formulae are shown below.

$$B = 7.3 \quad (29)$$

for  $K^- p$  scattering and

$$B = -24.3 + 7.0 \ln (s + 50.0) \quad (30)$$

for  $K^+ p$  interaction. The square of the momentum transfer  $t (GeV/c)^2$ , and the invariant mass squared,  $s (GeV/c)^2$ , are two convenient Mandelstam variables.

Our parameterized formulae,  $\alpha$ , for  $K^- p$  and  $K^+ p$  scattering, respectively, are as follows.

$$\alpha = - \frac{0.32}{1.0 + 0.9P_K^{Lab^2}} \sin \left\{ \frac{5\pi}{2} (P_K^{Lab} - 0.2) \right\} \quad (31)$$

for  $K^- p$  scattering and

$$\alpha = -1.86e^{-(P_K^{Lab} - 0.1)^2/0.41} - 0.44 \quad (32)$$

for  $K^+ p$  interaction where  $P_K^{Lab}$  is the kaon laboratory momentum in  $GeV/c$ .

The total and absorptive cross sections for  $K^\pm - A^{127}$  scattering using the harmonic well and Woods-Saxon single particle densities are shown in Figs. 7 and 8. Although we cannot evaluate the exact error due to the scarcity of experimental data, we expect that our calculation reasonably represents the situation, because of the good agreement between our calculation and the experimental data of other quantities such as the differential cross sections of kaon-proton and kaon-nucleus scattering.

In case of  $K^+ p$  scattering our scattering amplitude was quite reasonable. Moreover, the calculation of the differential cross section gave us more accurate result as the energy of projectile went higher. For  $K^\pm - C^{12}$  scattering the differential cross sections are estimated lower than the experimental results. It may be natural because we used a very simplified, non-relativistic optical potential. At the very forward angle the experiments show us the differential cross sections rise very rapidly, but the calculations converge smaller values. This comes from the fact that we have neglected the contribution of Coulomb interaction which is the long range interaction in the optical potential.

The total and absorptive cross sections for  $K^-$  - nucleus scattering were bigger than those of  $K^+$  - nucleus scattering. This, of course, indicates that  $K^-$  meson interacts with nucleons stronger than  $K^+$  meson. According to the quark model,  $K^+$  resonant peak requires the formation of five-quark

objects which have never been found, but the  $K^- N$  interactions are so strong that the cross sections are roughly comparable to those of nucleon-nucleon scattering.

$K^+$  -nucleus total cross section shows almost perfect linear dependence of  $A$  and  $K^-$  - nucleus total cross section also represents linearity of  $A$  at high energies, but exhibits a little complexity at low energies. Other things that we can give attention to are that the absorptive cross section of  $K^+$  - nucleus scattering depends on  $A^{0.82}$  linearly, but  $K^-$  - nucleus absorptive cross section does not show fairly good linear dependence of  $A^{0.82}$  as in the case of total cross section at relatively low energies. The linear dependence of  $A^{0.82}$  of absorptive cross section tells us that the nucleus is not perfectly black to the kaon projectile.

The results of this work will be used in the hadron transport computer code at NASA Langley Research Center (Ref. 18).

## References

1. Watson, K.M., Phys. Rev. 1953, **89**, 575
2. Frank, R.M.; Gammel, J.L.; Watson, K.M., Phys. Rev. 1956, **101**, 891
3. Watson, K.M., Phys. Rev. 1957, **105**, 1388
4. Wilson, J.W., A Dissertation for Ph.D, 1975
5. Wilson, J.W.; Phys. Lett. B 1974, **52**, 149
6. Wilson, J.W.; Townsend, L.W., Can. J. Phys. 1981, **59**, 1569
7. Buck, W.W.; Norbury, J.W.; Townsend, L.W.; Wilson, J.W., Phys. Rev. C 1986, **33**, 234
8. Aguilar-Benitez, M. *etal.*, "Particle Properties Data Booklet", North-Holland, Amsterdam, April 1986
9. Marlow, D.; Varnes, P.D.; Colella, N.J.; Dytman, S.A.; Eisenstein, R.A.; Grace, R.; Takeuchi, F.; Wharton, W.R.; Bart, S.; Hancock, D.; Hackenberg, R.; Hungerford, E.; Mayes, W.; Pinsky, L.; Williams, T.; Chrien, R.; Palevsky, H.; Sutter, R., Phys. Rev. C 1982, **25**, 2619
10. Siegel, P.B.; Kaufmann, W.B.; Gibbs, W.R., Phys. Rev. C 1984, **30**, 1256
11. Goldberger, M.L.; Watson, K.M., "Collision Theory", John Wiley & Sons, New York, 1964
12. Borkowski, F.; Simon, G.G.; Walther, V.H.; Wendling, R.D., Z. Phys. A 1975, **275**, 29
13. Price, LeRoy R.; Barash-Schmidt, Naomi; Benary, Odette; Bland, Roger W.; Rosenfeld, Arther H.; Wohl, Charles G., "A Compilation of  $K^+ N$  Reactions", Lawrence Radiation Laboratory, University of California, Berkley, California, UCRL-20000  $K^+ N$ , Sept. 1969

14. Giacomeli, G., "Total Cross Section Measurement", Pergamon Press, Ltd, New York, 1970
15. Baldini, A.; Flaminio, V.; Moorehead, W.G.; Morrison, D.R.O., Landolt-Börnstein New Series I/12a and I/12b, "Total Cross-Sections for Reactions of High Energy Particles", Springer Berlin Heidelberg, 1988
16. Perl, Martin L., "High Energy Hadron Physics", John Wiley & Sons, Inc., 1974
17. Lusiguoli, M.; Restignoli, M.; Violini, G.; Snow, G.A., Nuovo Cimento 1966, **45**,A792
18. Wilson, J.W.; Townsend, L.W.; Chun, S.Y.; Lamkin, S.L.; Ganapol, B.D.; Hong, B.S.; Buck W.W.; Khan, F.; Cucinotta, F.A.; Nealy, J.E., "BRYNTRN; A baryon transport model", NASA TP-2887, Feb. 1989.

Table I.

Nuclear charge distribution parameters from electron scattering data taken from Ref. 8.

Nucleus	Distribution	$\gamma$ or $t_c$ (fm)	$a$ or $R$ (fm)
$H^2$		0	1.71
$He^4$	HW	0	1.33
$Li^7$	HW	0.327	1.77
$Be^9$	HW	0.611	1.791
$B^{11}$	HW	0.811	1.69
$C^{12}$	HW	1.247	1.649
$N^{14}$	HW	1.291	1.729
$O^{16}$	HW	1.544	1.833
$Ne^{20}$	WS	2.517	2.74
$Al^{27}$	WS	2.504	3.05
$Ar^{40}$	WS	2.693	3.47
$Fe^{56}$	WS	2.611	3.971
$Cu^{64}$	WS	2.504	3.05
$Br^{80}$	WS	2.306	4.604
$Ag^{108}$	WS	2.354	5.139
$Ba^{138}$	WS	2.621	5.618
$Pb^{208}$	WS	2.416	6.624

Table II.  
Kaon-nucleon total cross section parameters

	$i$	$PR_i$ (GeV/c)	$m_i$ (mb)	$n_i$ (GeV/c)
$K^-p$	1	0.8	11.	0.21
	2	1.05	27.	0.2
	3	1.60	9.	0.35
	4	2.30	4.	1.
	5	3.50	4.30	2.
$K^+p$	1	0.80	-4.	0.40
	2	1.30	2.50	1.

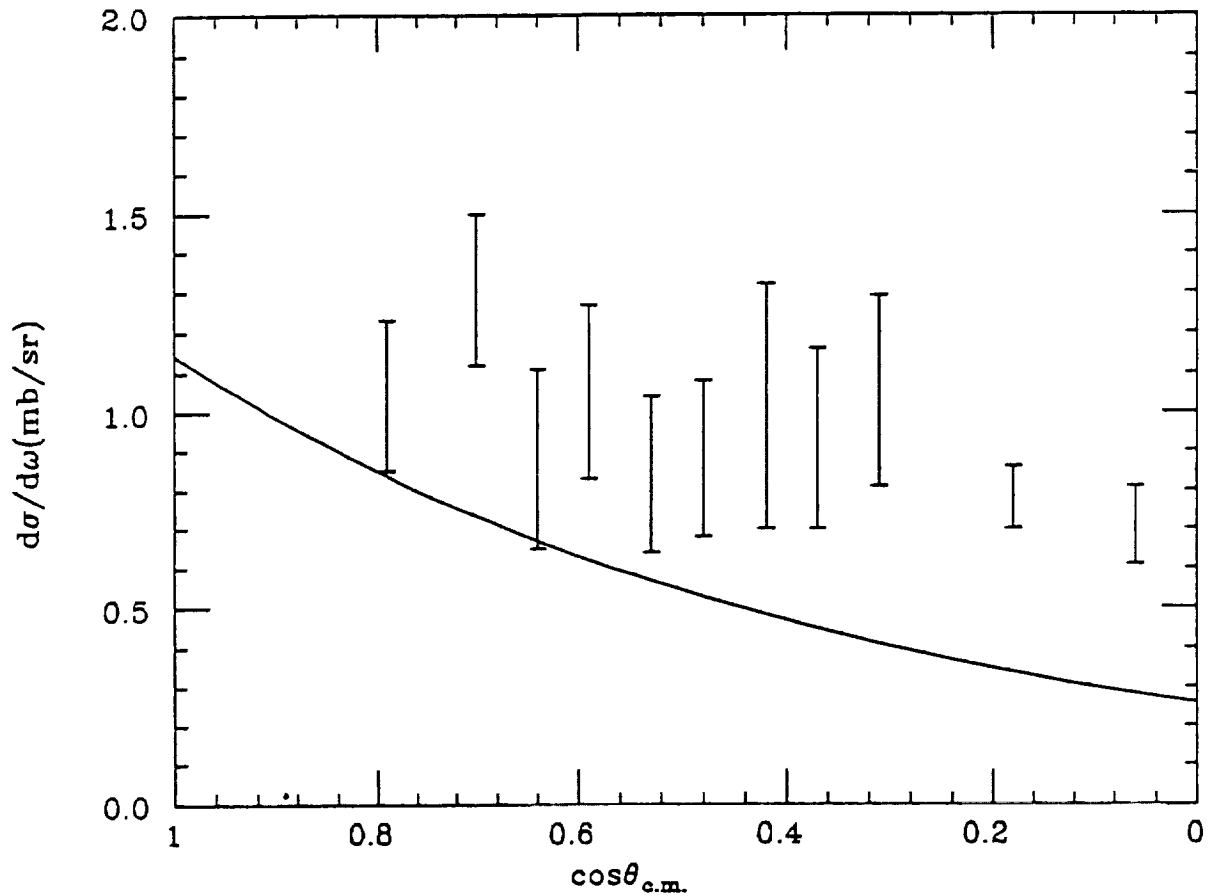


Figure 1. Differential cross section of  $K^+p$  scattering at 503 MeV

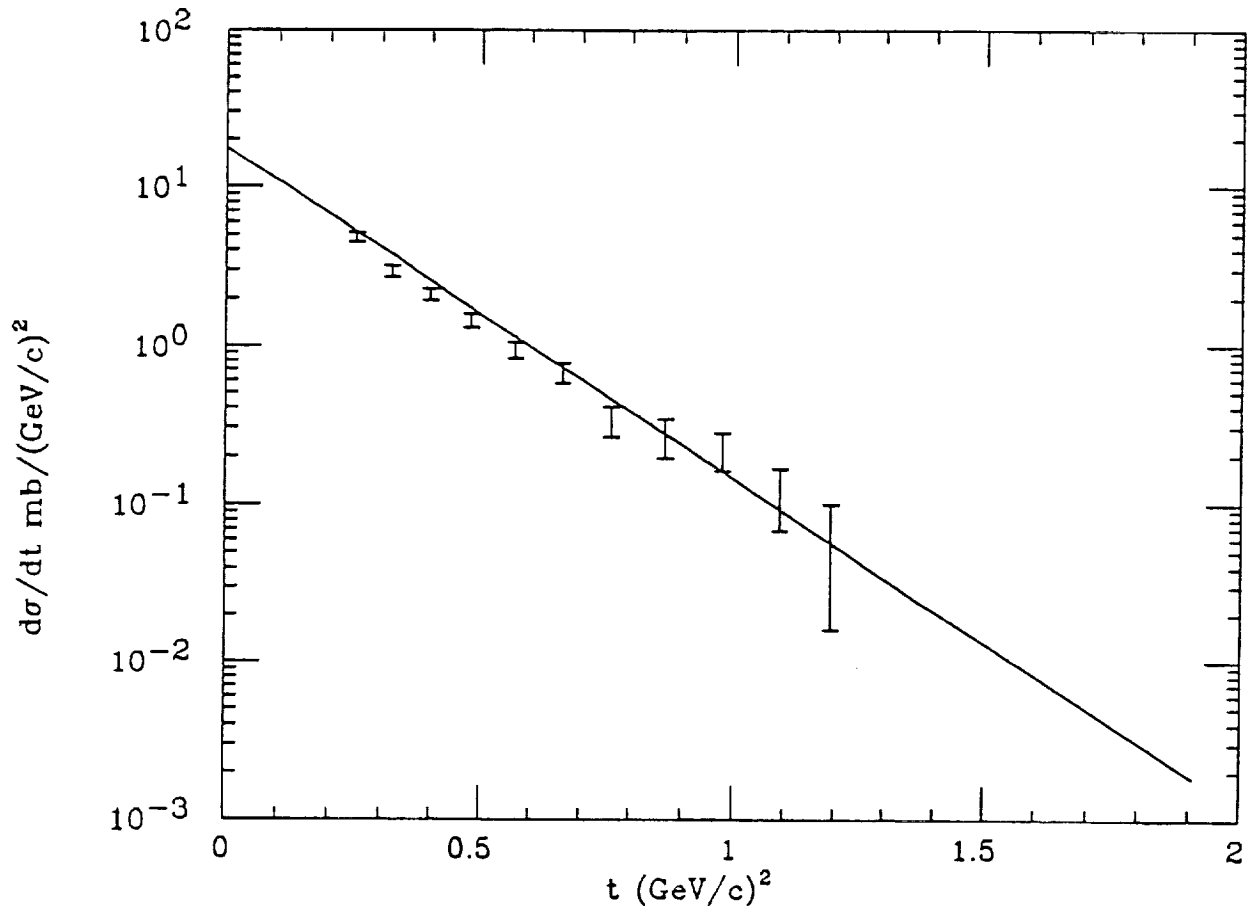


Figure 2. Differential cross section of  $K^+p$  scattering at 6324.9 MeV

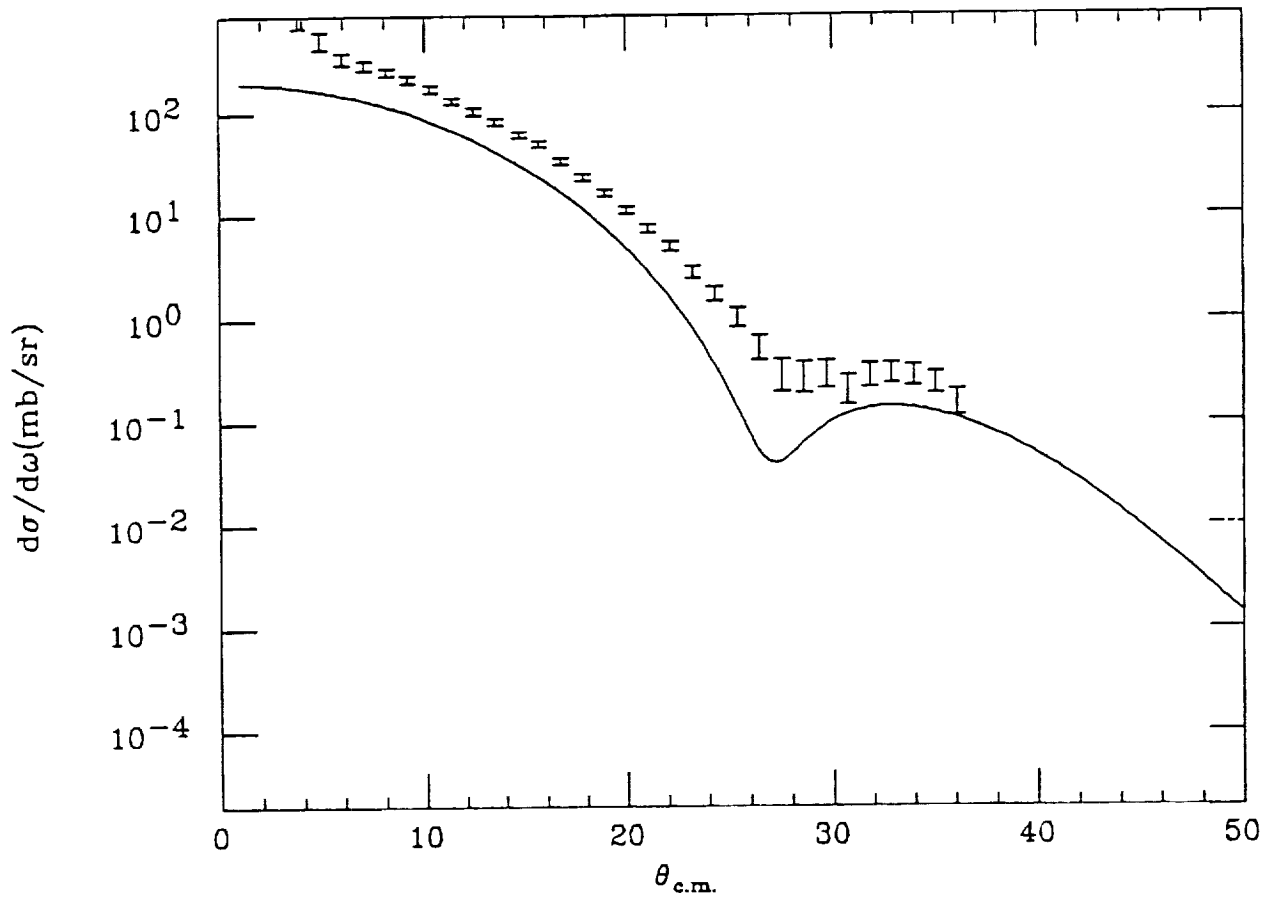


Figure 3. Differential cross section of  $K^+C^{12}$  scattering at 800 MeV/c

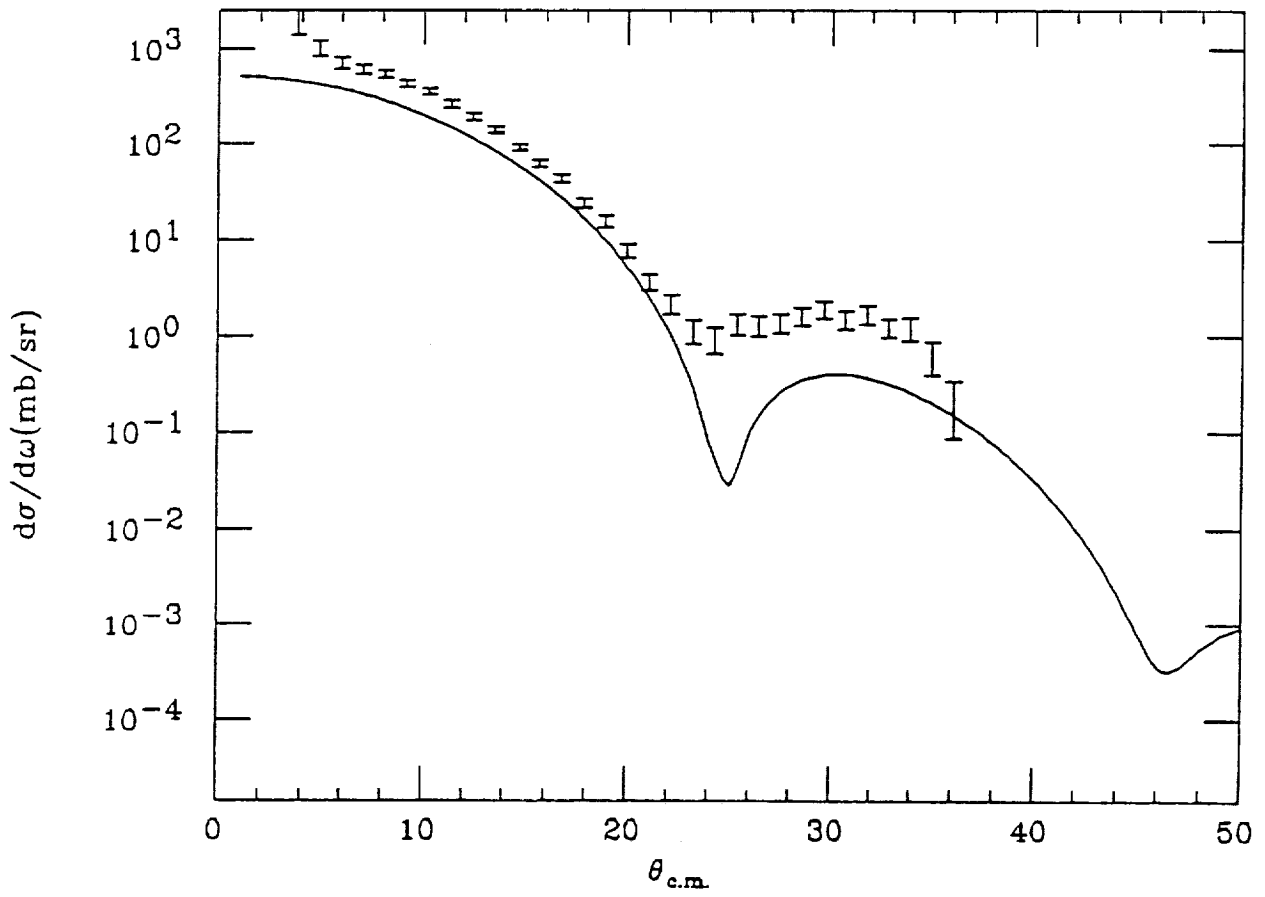


Figure 4. Differential cross section of  $K^-C^{12}$  scattering at 800 MeV/c

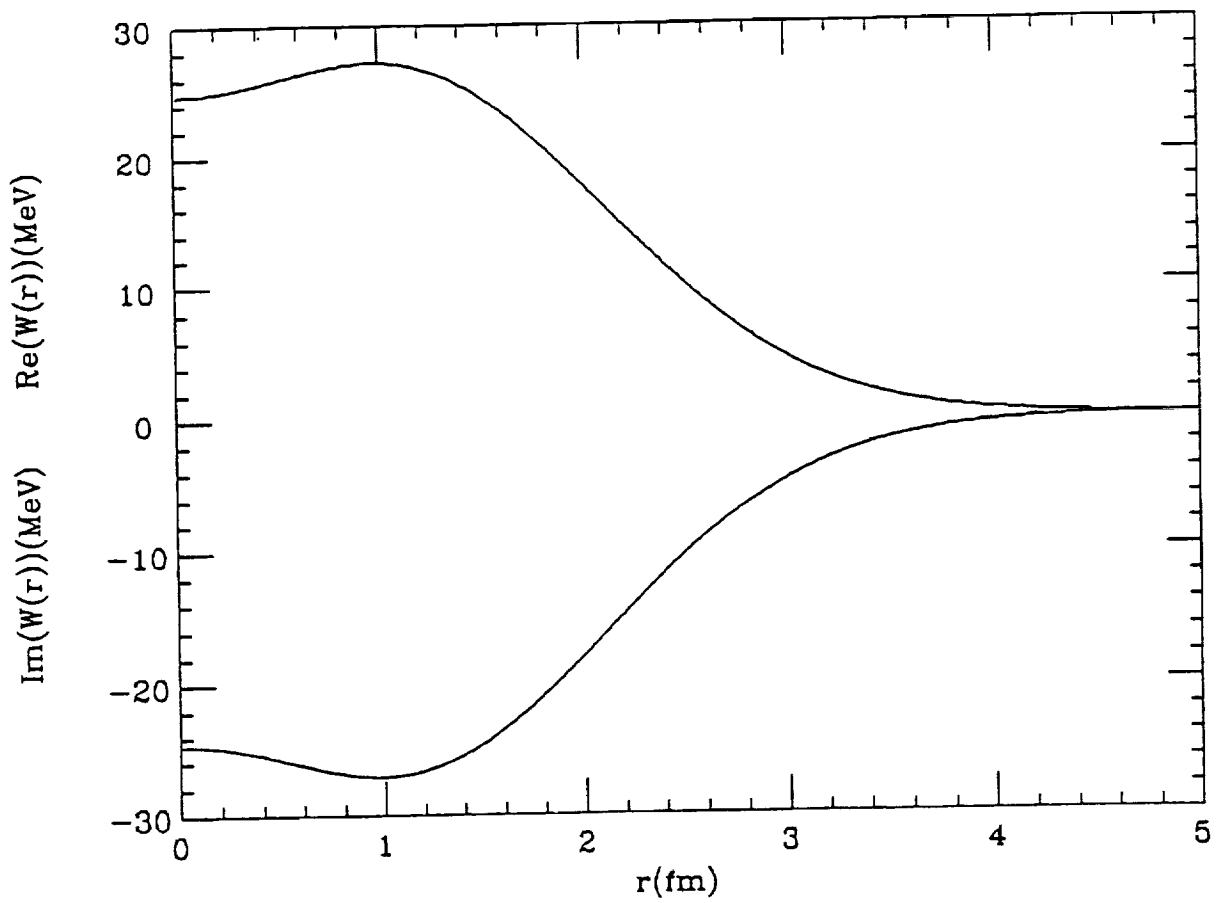


Figure 5. Optical potential for  $K^+ C^{12}$  at  $800 \text{ MeV}/c$

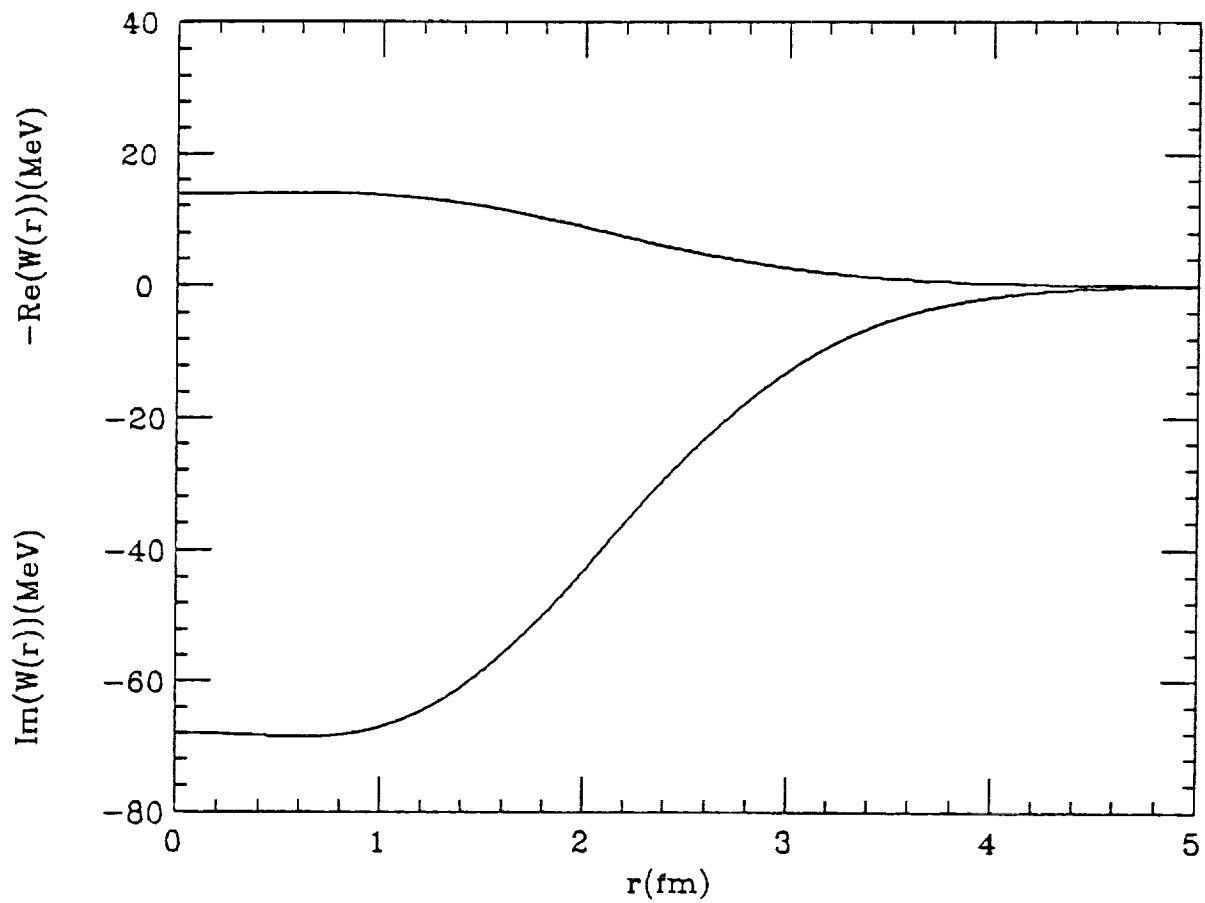


Figure 6. Optical potential for  $K^- C^{12}$  at  $800 \text{ MeV}/c$

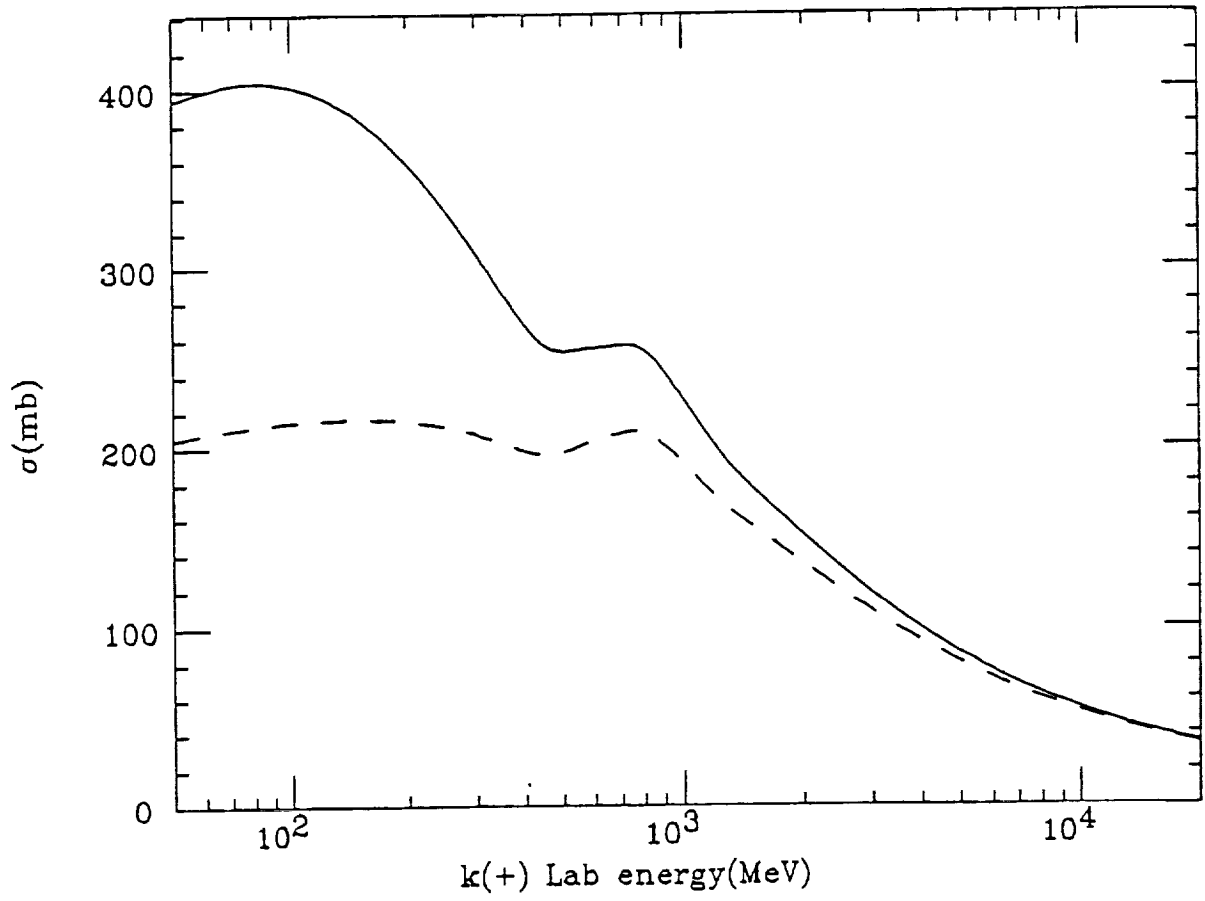


Figure 7. Total (solid) and absorptive (dashed) cross sections for  $K^+ Al^{27}$

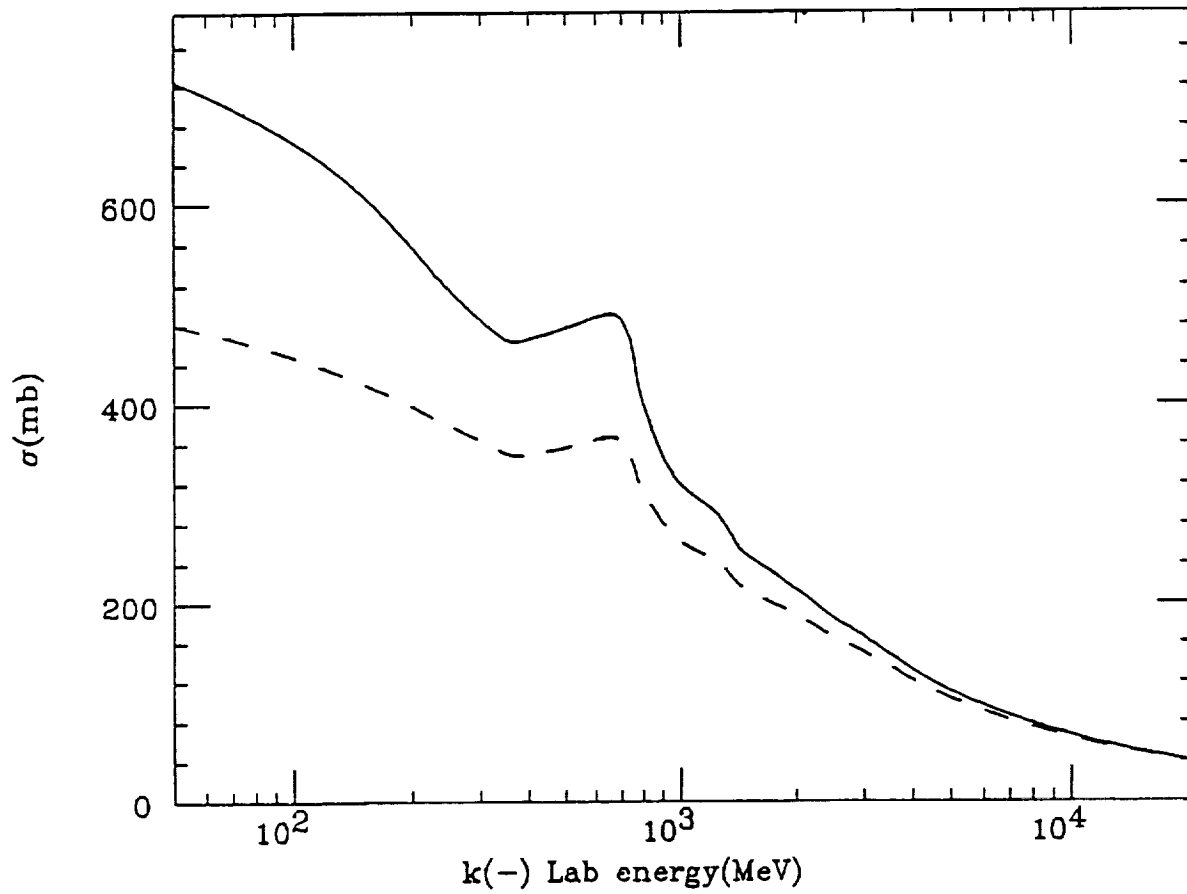


Figure 8. Total (solid) and absorptive (dashed) cross sections for  $K^- Al^{27}$